Gravitational-Wave Fringes at LIGO: Detecting Compact Dark Matter by Gravitational Lensing

Sunghoon Jung[1,*] and Chang Sub Shin[2]
[1]Center for Theoretical Physics, Department of Physics and Astronomy, Seoul National University, Seoul 08826, Korea
[2]Center for Theoretical Physics of the Universe, IBS, Daejeon 34051, Korea

(Received 13 December 2017; revised manuscript received 31 July 2018; published 30 January 2019)

Utilizing gravitational-wave (GW) lensing opens a new way to understand the small-scale structure of the Universe. We show that, in spite of its coarse angular resolution and short duration of observation, LIGO can detect the GW lensing induced by small structures, in particular by compact dark matter (DM) or the primordial black hole of 10–10^5 $M_\odot$, which remains an interesting DM candidate. The lensing is detected through GW frequency chirping, creating the natural and rapid change of lensing patterns: frequency-dependent amplification and modulation of GW waveforms. As a highest-frequency GW detector, LIGO is a unique GW lab to probe such light compact DM. With the design sensitivity of Advanced LIGO, one-year observation by three detectors can optimistically constrain the compact DM density fraction $f_{\rm DM}$ to the level of a few percent.

DOI: 10.1103/PhysRevLett.122.041103

Introduction.—The GW from far-away binary mergers [1,2] is a new way to see the Universe with gravitational interaction. Not only is it revealing astrophysics of solar-mass black holes and neutron stars, but the GW can also carry information of intervening masses and the evolution of the Universe through gravitational lensing. Having the long wavelength λ, the GW is usually expected to be lensed by heaviest structures (such as galaxies and their clusters) with large enough Schwarzschild radii, $2GM/c^2 = 2M \gg \lambda \simeq 2\times 10^3(100\ \mathrm{Hz}/f)M_\odot$. Their prototypical lensing signal is strongly time-delayed GW images [3,4] or statistical correlations [5].

In this Letter, we show that LIGO can detect the GW lensing induced by much lighter compact structures. The new lensing observable depends crucially on the GW frequency evolution during binary inspiral—"chirping." The chirping provides the natural and rapid change of lensing patterns so that LIGO can detect relatively weak GW lensing, in spite of its coarse angular resolution [$\mathcal{O}$(1–10) deg [6,7], let alone typical strong-lensing image separations of arcsec] and short measurement time (less than minutes, let alone typical microlensing observations of a few weeks). Remarkably, measuring highest frequencies of $f = 10$–5000 Hz, LIGO is a unique GW detector to see compact structures as light as $M = 10$–10^5 $M_\odot$.

An important example of such light structure is the compact DM. It remains an attractive DM candidate, predicted by various models of particle physics and cosmology: axion miniclusters, compact mini halos, and primordial black holes [8–19]. Compact DM is mainly searched by light lensing: microlensing (temporal variation of brightness) [20,21] and strong lensing (multiple images) [22,23]. But, in a wide range of compact DM mass 10^{-16}–10^5 $M_\odot$, its density fraction $f_{\rm DM} \lesssim 0.1$–1 of total DM density remains to be probed [24]. We present the prospect for the new LIGO lensing observable to probe the compact DM of $M_{\rm DM} = 10$–10^5 $M_\odot$.

GW lensing observable.—The proposed GW lensing observable relies on the following properties (in contrast to those of light).

Above all, the binary GW frequency chirps. Suppose that some lensing creates two GW images with (small) time-delay Δt_d. The two images interfere since LIGO cannot resolve them. Then, the phase shift between them $\sim f\Delta t_d$ grows with the frequency, and the resulting interference pattern *changes* with chirping [25,26] (see Fig. 1 dashed)—frequency-dependent modulation. The final stage of binary inspiral (observed by LIGO) is where the frequency-dependent signal can be detected most efficiently because the frequency is highest and grows most rapidly.

Second, the GW wavelength is much longer than that of light. Therefore, GW lensing does not always produce two images with constant time delay. In general, the lensed GW waveform $\tilde{h}^L(f)$ is a superposition of all unlensed waveforms $\tilde{h}(f)$ that follow all possible null rays (passing $\vec{\theta}$ in the thin lens plane at redshift $z_{\rm DM}$) [27,28],

$$\tilde{h}(f)^L = \frac{d_L d_S(1+z_{\rm DM})}{i d_{LS}} f \int d^2\vec{\theta}\exp[i2\pi f\Delta t(\vec{\theta},\vec{\theta}_s)]\tilde{h}(f), \tag{1}$$

with $d_{L,S,LS}$ the angular-diameter distance to the lens, source, and between them; the compact DM is treated

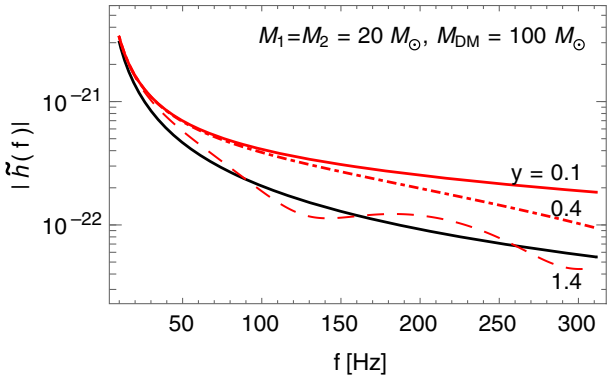

FIG. 1. Illustration of GW lensing fringe at aLIGO: Lensed (red curves) vs unlensed (black curve) waveforms. The lensing compact DM mass $M_{\rm DM} = 100\ M_\odot$ and redshifted GW binary masses $M_1 = M_2 = 20\ M_\odot$ merging at $f \simeq 320$ Hz. At small impact angle $y = \theta_s/\theta_E$ (red-solid line) Eq. (1), frequency-dependent amplification cannot be fit by a constant rescaling A_0 [Eq. (4)] of unlensed waveforms (black curve); whereas, at large y (dashed line), frequency-dependent modulation cannot be matched by a constant phase shift ϕ_0 [Eq. (3)]. In general (dot dashed curve), both lensing effects coexist.

as a point lens [27,28] with the time-delay $\Delta t(\vec{\theta},\vec{\theta}_s) = (1+z_{\rm DM})[(d_L d_S/2d_{LS})|\vec{\theta}-\vec{\theta}_s|^2 - 4M_{\rm DM}|\vec{\theta}|]$ and the source impact angle $y = \theta_s/\theta_E$ normalized by the Einstein angle $\theta_E = \sqrt{(4GM_{\rm DM}/c^2)(d_{LS}/d_L d_S)}$. Only when the GW frequency is larger than the inverse of the typical time delay between null rays $f\Delta t_d \simeq 4fM_{\rm DM} \simeq 2\times 10^{-5}(M_{\rm DM}/M_\odot)(f/{\rm Hz}) \gg 1$ (equivalently, $\lambda \ll M_{\rm DM}$), the integral is dominated by discrete stationary points with separate images (geometric optics limit). In the opposite limit, GW diffraction becomes important and lensing amplification becomes weaker (wave optics limit); eventually, the GW does not see the lens if its wavelength becomes too long.

In particular, the GW wavelength in the LIGO band, $\lambda \simeq 2\times 10^3 (100\ {\rm Hz}/f)\, M_\odot$, is comparable to the Schwarzschild radius of the compact DM with $M_{\rm DM} =$ 10–$10^5\ M_\odot$. Chirping from 10 Hz to $\mathcal{O}$(100–1000) Hz, GW lensing by such masses may transition from wave optics [$\lambda_{\rm GW} \gtrsim \mathcal{O}(M_{\rm DM})$] to geometric optics [$\lambda_{\rm GW} \lesssim \mathcal{O}(M_{\rm DM})$]. Therefore, with chirping, GW lensing magnitude (both amplification and time delay) also grows; compare the low and high frequency regions in Fig. 1.

The two effects combined—frequency-dependent amplification and modulation—define our "GW fringe" lensing signal. Figure 1 illustrates fringes in comparison to the unlensed waveform. Below, we will calculate the fringe detection efficiency at LIGO, lensing optical depth, detection rate, and expected constraints on $f_{\rm DM}$.

Analysis for lensing detection.—In the LIGO frequency band, binary GWs spend only a few seconds or minutes. Therefore, a detector on Earth is almost at rest during the measurement. Then, the unlensed GW waveform is sinusoidal when observed by a single LIGO detector

$$\begin{aligned} h(t) &= A_+(t)F_+\cos\phi(t) + A_\times(t)F_\times \sin\phi(t) \\ &= A(t)\cos[\phi(t)+\phi_0], \end{aligned} \tag{2}$$

with detector response functions $F_{+,\times}$ constant in time during the measurement period. Rather, the time dependences of amplitude $A(t)$ and phase $\phi(t)$ are determined uniquely by the redshifted chirp mass $\mathcal{M}_z = [M_1^3 M_2^3/(M_1+M_2)]^{1/5}$ (with redshifted $M_1 = M_2$ in this work): $A(t) \propto \mathcal{M}_z^{5/3} f(t)^{2/3}$ with $f'(t) = (96/5)\pi^{8/3} f(t)^{11/3}\mathcal{M}_z^{5/3}$ at the leading Newtonian order, where $f(t) \equiv \phi'(t)/2\pi$ is the instantaneous GW frequency.

Now, the unlensed waveform observed in the frequency domain is simply

$$\tilde{h}(f) = \tilde{A}(f)\exp\{i[\Psi(f)+\phi_0]\}, \tag{3}$$

where

$$\tilde{A}(f) = A_0 \mathcal{M}_z^{5/6} f^{-7/6}, \tag{4}$$

$$\Psi(f) = 2\pi f t_c + \frac{3}{128}(\pi \mathcal{M}_z f)^{-5/3}, \tag{5}$$

and any constant phase shift is absorbed into ϕ_0. Although the real-valued constant A_0 depends on various source parameters (such as polarization and distance), single short measurement can only measure A_0. For simplicity, we ignore higher-order post-Newtonian terms, spin effects, orbital eccentricity, and nonquadrupole modes; see Ref. [29] for caveats.

We use the χ^2 least-squares fit method to determine whether GW lensing can be detected [30]. We define the goodness of fit of (trial) unlensed waveforms to the (observed) lensed waveform as

$$({\rm SNR}_{\rm test})^2 \equiv 4\int_{f_0}^{f_1} \frac{|\tilde{h}(f)^L - \tilde{h}(f)_{\rm best-fit}|^2}{S_n(f)} df, \tag{6}$$

similarly to the observed signal-to-noise ratio (SNR)

$$({\rm SNR})^2 = 4\int_{f_0}^{f_1} \frac{|\tilde{h}(f)^L|^2}{S_n(f)} df. \tag{7}$$

The integration is done over the aLIGO frequency band [31]: $f_0 = 10$ Hz, $f_1 = \min(f_{\rm cut}, 5000\ {\rm Hz})$, where the cutoff frequency $f_{\rm cut} = [3\sqrt{3}\pi(M_1+M_2)]^{-1}$ at $r = 3(M_1+M_2)$ [32].

For the given observed lensed waveform $\tilde{h}(f)^L$, we find the best-fit unlensed waveform $\tilde{h}(f)_{\rm best-fit}$ by minimizing ${\rm SNR}_{\rm test}$ over two fitting parameters, A_0 and ϕ_0. Here, we assume that the chirp mass $\mathcal{M}_z$ and the coalescence time t_c (time at which f formally diverges) are well measured regardless of lensing effects [34] (but see also, e.g., Refs. [35,36]). The simplified best fit based on A_0 and ϕ_0 is convenient to capture the leading physics of

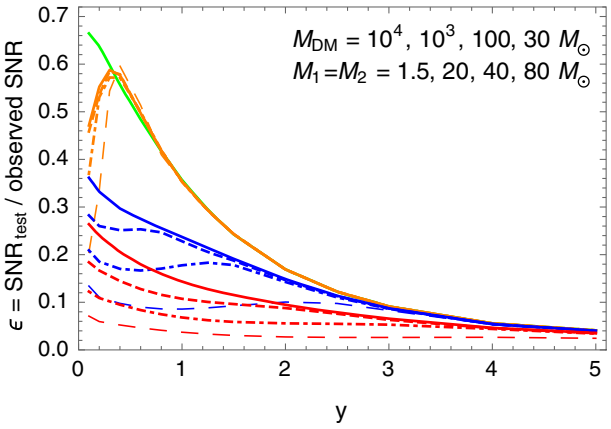

FIG. 2. The lensing-detection efficiency ϵ in Eq. (8) of a single aLIGO detector with design sensitivity. The DM masses are $M_{\rm DM} = 10^4$ (green), 10^3 (orange), 100 (blue), 30 (red) $M_\odot$ and redshifted binary masses $M_1 = M_2 = 1.5$ (solid line), 20 (dashed line), 40 (dot-dashed line), 80 (long-dashed line) $M_\odot$.

GW fringe, as illustrated in Fig. 1, but see Ref. [29] for caveats.

We regard that the existence of GW lensing is detected if $\mathrm{SNR}_{\rm test} \geq 3$ or 5 with $\mathrm{SNR} \geq 8$ [37]. With multiple detectors, we require the total SNR quadrature sum to satisfy these criteria. In Fig. 2, we show the lensing-detection efficiency of the single aLIGO detector defined as

$$\epsilon \equiv \frac{\mathrm{SNR}_{\rm test}}{\mathrm{SNR}}. \tag{8}$$

It is typically $\sim\mathcal{O}(10)\%$ so that strong GWs with $\mathrm{SNR} \sim \mathcal{O}(10)$ can be lensing detected with $\mathrm{SNR}_{\rm test} \sim \mathcal{O}(1)$. The heavier the lens, the larger ϵ, trivially. The lighter GW binaries, the larger ϵ because lighter GWs merge at higher frequencies experiencing more modulation.

The slight fluctuation and drop of the ϵ curve in Fig. 2 are related to the interplay of frequency-dependent modulation and amplification. The former becomes more significant at large y due to larger time delay, whereas the latter at small y due to stronger lensing; see Fig. 1. Intermediate regimes may produce less exotic waveforms (e.g., dot-dashed curve in Fig. 1), if the GW merges just before the first destructive interference.

Advanced LIGO prospects.—We turn to discuss expected results from three aLIGO detectors, representing a network of future detectors. We assume design aLIGO sensitivity (the dark-blue noise curve in Fig. 1 of Ref. [31] and horizon in Ref. [33]), yielding $\sim$3 times larger SNR (seeing $\sim$3 times farther distance) than current LIGO.

The differential optical depth for *detectable* lensing for the given lensing parameters (source and lens masses and locations—$\mathcal{M}_z$, z_S and $M_{\rm DM}$, $z_{\rm DM}$, y) is

$$\frac{d^2\tau}{dy dz_{\rm DM}} = \frac{ca(z_{\rm DM})}{H(z_{\rm DM})} 2\pi (d_L\theta_E)^2 y (1+z_{\rm DM})^3 n_{\rm DM} P(w)$$
$$= \frac{3}{2} f_{\rm DM}\Omega_{\rm DM} \frac{H_0^2(1+z_{\rm DM})^2}{H(z_{\rm DM})c} \frac{d_L d_{LS}}{d_S} 2yP(w), \tag{9}$$

where a constant comoving lens density $n_{\rm DM}$ is assumed for the compact DM mass density $f_{\rm DM}\Omega_{\rm DM}$. The optical depth depends on the detectability. The parameter-dependent detection efficiency ϵ [Eq. (8)] determines the minimum SNR needed for detectable lensing: $\max(8, 3/\epsilon$ or $5/\epsilon)$ depending on the $\mathrm{SNR}_{\rm test} > 3$ or 5 criteria. Then, among the sources with randomly chosen sky position, inclination, and polarization angle, the probability for SNR to be greater than the minimum value is denoted by $P(w)$ with $w = (\mathrm{SNR\ needed})/(\mathrm{SNR\ optimal})$, where (SNR optimal) is the maximum possible SNR for some optimally oriented source. $P(w)$ is the cumulative distribution of w spanned by such random source parameters; $P(w) = 1$ for $w = 0$, and decreases to $P(w) = 0$ for $w > 1.4$ for three detectors [38]. The probability is convoluted with comoving volume and lens density to yield the optical depth τ (for the given $\mathcal{M}_z$, z_S and $M_{\rm DM}$). We assume a standard cosmology with the Hubble parameter $H(z)$, mass density fractions $\Omega_m = 0.27$, $\Omega_{\rm DM} = 0.24$, $\Omega_\Lambda = 0.73$ for matter, DM, and cosmological constant.

The source distribution—the comoving merger-rate density $\dot{n}_{\rm merger}$—is assumed to be constant in z_S for simplicity [39], but its dependence on $\mathcal{M}_z$ is kept. Two sets of distributions on $\mathcal{M}_z$ are taken from Ref. [40]: the optimistic merger model $M1$ predicting highest merger rate consistent with LIGO's observations, and the pessimistic model $M3$. For the given masses $\mathcal{M}_z$ and $M_{\rm DM}$, the $\dot{n}_{\rm merger}(\mathcal{M}_z)$ yields the merger rate $\dot{N}_{\rm merger}(\mathcal{M}_z) = \int dV_{\rm com}\dot{n}_{\rm merger}(\mathcal{M}_z)$ and, finally, the detectable lensing rate as

$$\dot{N}_{\rm lensing}(\mathcal{M}_z, M_{\rm DM}) = \int dV_{\rm com}\dot{n}_{\rm merger}\tau(z_S), \tag{10}$$

where $\tau(z_S) = \int_0^{z_S} dz_{\rm DM} \int dy (d\tau/dy dz_{\rm DM})$ and the comoving volume element $dV_{\rm com} = [4\pi\chi(z_S)^2 c/H(z_S)]dz_S$ in terms of the comoving distance χ.

In Fig. 3, we show the ratio of detectable lensing to the total merger as the volume-averaged optical depth (again for the given masses $\mathcal{M}_z$ and $M_{\rm DM}$)

$$\bar{\tau}(\mathcal{M}_z, M_{\rm DM}) \equiv \frac{\dot{N}_{\rm lensing}}{\dot{N}_{\rm merger}} = \frac{\int dz_S \frac{4\pi\chi(z_S)^2 c}{H(z_S)} \tau(z_S)}{\int dz_S \frac{4\pi\chi(z_S)^2 c}{H(z_S)}}. \tag{11}$$

The averaged optical depth $\bar{\tau}$ is a function (only) of $\mathcal{M}_z$ and $M_{\rm DM}$. It is smallest for lightest binaries mainly because GWs are weakest. It becomes largest at $\mathcal{M}_z \sim 30\ M_\odot$ for light $M_{\rm DM}$ as ϵ is smaller for heavier binaries, whereas it

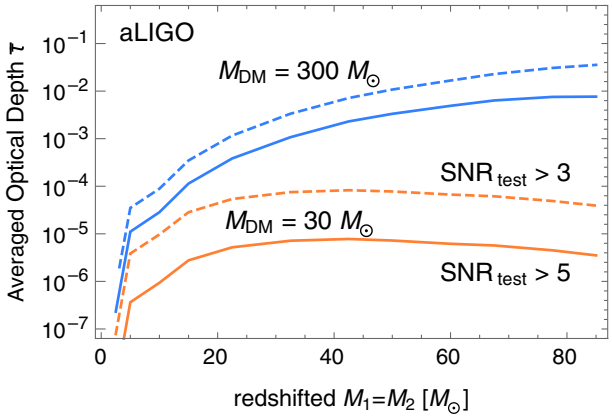

FIG. 3. The volume-averaged optical depth $\bar{\tau}$ as defined in Eq. (11). It is the probability for detectable lensing, including the probability for $\mathrm{SNR}_{\mathrm{test}} > 3$ (dashed line) or 5 (solid line) and SNR > 8 from three aLIGOs. The upper (lower) set of curves is for $M_{\mathrm{DM}} = 300(30)\ M_\odot$. $f_{\mathrm{DM}} = 1$.

keeps growing for heavy M_{DM} since ϵ depends less on the binary mass; see Fig. 2.

Shown in Fig. 4 is the final lensing detection rate, $\dot{N}_{\mathrm{lensing}}$ in Eq. (10), from three aLIGO detectors. The highest detection rate is expected from $\mathcal{M}_z = 20$–$30\ M_\odot$, as $\bar{\tau}$ is typically largest there. The total expected yearly detections are sizable: optimistically, 6 (170) for $M_{\mathrm{DM}} = 30(300)\ M_\odot$ with $\mathrm{SNR}_{\mathrm{test}} > 3$ and 0.6 (55) with $\mathrm{SNR}_{\mathrm{test}} > 5$. Pessimistic expectations are about 25–40 times smaller.

Based on the Poisson distribution of the number of fringe detections, we calculate the value of f_{DM} giving 95% probability of one detection, shown in Fig. 5 as 95% C.L. constraints on f_{DM} assuming null detections. But a proper characterization of the probability distribution will be needed to derive more realistic constraints. The sensitivities start from $M_{\mathrm{DM}} \sim 10\ M_\odot$, become strongest for $M_{\mathrm{DM}} \gtrsim 10^2\ M_\odot$, and stop shown for $M_{\mathrm{DM}} \gtrsim 10^5\ M_\odot$. The three regions have different values of the phase shift

$$f\Delta t_d \simeq 2 \times 10^{-5}\ (M_{\mathrm{DM}}/M_\odot)(f/\mathrm{Hz}) \qquad (12)$$

(in the wave-optics regime, we can think of Δt_d as a typical time delay from null rays with $\theta \simeq \theta_E$).

For $f\Delta t_d \gtrsim 0.1$ from $M_{\mathrm{DM}} \gtrsim 10^2\ M_\odot$, the GW fringe is most pronounced, and the LIGO fringe search is a powerful probe of those compact DM. Here, the $\mathcal{O}(1)$ evolution of the frequency in the LIGO band produces $\gtrsim\mathcal{O}(1)$ cycles of fringe patterns, which is easiest to detect. Resulting optimistic sensitivity $f_{\mathrm{DM}} \lesssim 10^{-2}$ is comparable to or stronger than existing constraints from mircolensing [21], millilensing [23], a star's caustic crossing [41,43,44], and star-cluster survival [42] as well as various proposed searches [45,46]. The GW fringe sensitivity will further improve with longer observation time.

The strong sensitivity is attributed to high detection efficiencies ϵ and large merger rates. Not only can LIGO see sources at far distance ($z_S \lesssim 2$ in this Letter, but farther with future upgrades), but also at large y too. Remarkably, large $y \gtrsim 1.5$ can still lead to sizable efficiency $\epsilon = 5$–25% in Fig. 2. Although lensing is weak there, the GW *amplitude* modification can still be $\sim 10\%$ (4%) for $y = 3$ (5). Combined with frequency-dependent interference over a range of frequencies, this can lead to such sizable ϵ. On the contrary, light lensing is observed through its brightness (squared amplitude) features so that large-y lensing effects are hardly observable.

The constraints become almost constant for heavy masses $M_{\mathrm{DM}} \gtrsim 200\ M_\odot$ in Fig. 5 because the decrease

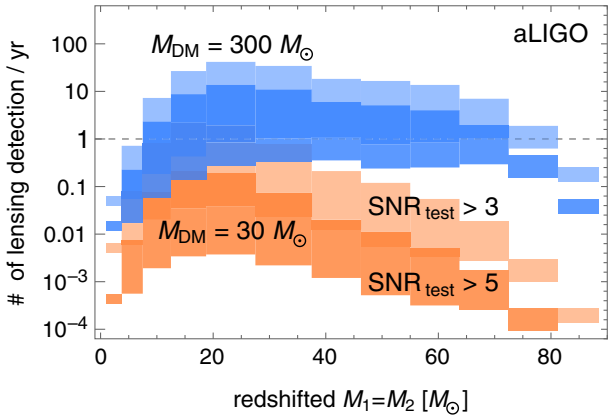

FIG. 4. The number of GW lensing detections per year by three aLIGOs. The darker (lighter) region satisfies $\mathrm{SNR}_{\mathrm{test}} > 5$ (3) and SNR > 8, and vertical ranges span between the optimistic merger-rate $M1$ and the pessimistic $M3$ [40]. The blue (orange) region is for the lensing $M_{\mathrm{DM}} = 300(30)\ M_\odot$. The horizontal dashed line denotes one detection per year. The total detection rate is the sum over mass bins. $f_{\mathrm{DM}} = 1$.

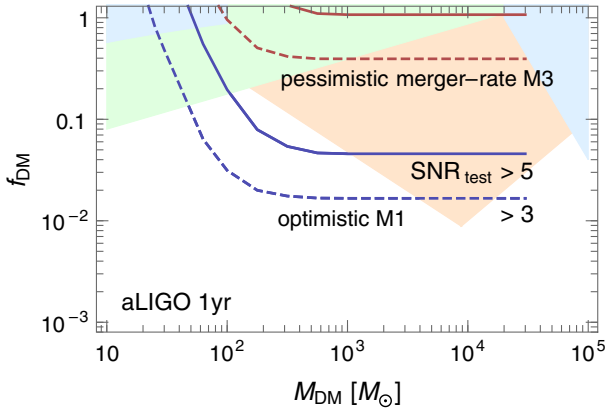

FIG. 5. Expected 95% C.L. constraints on f_{DM} from one-year observation by three aLIGOs. The Poisson distribution of fringe detection probability is assumed. $\mathrm{SNR}_{\mathrm{test}} > 3$ (dashed line) or 5 (solid line) is used with optimistic (blue) or pessimistic (red) merger-rate models. Shaded regions are existing constraints: microlensing (left blue) [21], caustic crossing (green) [41], cluster survival (orange) [42], and millilensing of quasars (right blue) [23].

of the DM number density (with heavier DM) is compensated by the increase of the Einstein radius in the last line of Eq. (9). Nevertheless, we stop showing the result at $M_{\rm DM} \sim 10^5\ M_\odot$, since waveform modulations with $f\Delta t_d \gtrsim 10^3$ in the heavy-$M_{\rm DM}$ region maybe too quick to be temporally resolved. On the other hand, LIGO fringe search is not sensitive to $M_{\rm DM} \lesssim \mathcal{O}(10)\ M_\odot$. Here, small phase-shift $f\Delta t_d \lesssim 0.1$ barely produces observable fringes.

In general, a lensing fringe becomes most pronounced when the following relation is satisfied:

$$(M_{\rm DM}/M_\odot)(f/{\rm Hz}) \gtrsim 10^4\text{–}10^6, \tag{13}$$

equivalent to $f\Delta t_d \gtrsim 0.1$–10 from Eq. (12). The maximum $f\Delta t_d$ (hence, $M_{\rm DM}f$) depends on the detector's temporal resolution, as discussed. But as a highest-frequency GW detector, LIGO can see the lightest DM; lower-frequency detectors (such as LISA) can probe only heavier DM. This discussion also applies to the photon fringe. The compact DM of 10^{-16}–$10^{-14}\ M_\odot$ is expected to produce (femtolensing) fringes on gamma-ray bursts (GRBs) with $f_{\rm GRB} \simeq 10\text{–}1000\ {\rm keV} \simeq 2.4 \times (10^{18}\text{–}10^{20})$ Hz [47], satisfying Eqs. (13) and (12). Although the GRB frequency does not change with time, a fringe spectrum can be observed [48].

Conclusion.—We have shown that LIGO can detect the GW lensing fringe induced by the compact DM of $M_{\rm DM} = 10\text{–}10^5\ M_\odot$. The LIGO measurement of GW fringes can surpass or strengthen existing constraints on such DM fraction, as shown in Fig. 5. Without LIGO fringe measurements, this small structure could not have been probed with GW. The general relation Eq. (13) suggests that lower-frequency detectors can probe heavier compact DM. Therefore, future broadband GW surveys covering $f = 10^{-9}$–10^3 Hz (from various detectors) are needed to probe a wide range of structures through the GW fringe.

We thank Hyung Mok Lee and Hyung Won Lee for useful comments. S. J. is supported by Korea NRF-2017R1D1A1B03030820 and NRF-2015R1A4A1042542. C. S. S. is supported by IBS under the project code IBS-R018-D1.

*sunghoonj@snu.ac.kr

[1] B. P. Abbott *et al.* (LIGO Scientific and Virgo Collaborations), Phys. Rev. Lett. **116**, 061102 (2016).
[2] B. P. Abbott *et al.* (LIGO Scientific and Virgo Collaborations), Phys. Rev. Lett. **119**, 161101 (2017).
[3] M. Sereno, A. Sesana, A. Bleuler, P. Jetzer, M. Volonteri, and M. C. Begelman, Phys. Rev. Lett. **105**, 251101 (2010).
[4] A. Pirkowska, M. Biesiada, and Z. H. Zhu, J. Cosmol. Astropart. Phys. 10 (2013) 022.
[5] P. Laguna, S. L. Larson, D. Spergel, and N. Yunes, Astrophys. J. **715**, L12 (2010).
[6] B. P. Abbott *et al.* (LIGO Scientific and VIRGO Collaborations), Living Rev. Relativity **19**, 1 (2016); **21**, 3 (2018).
[7] P. W. Graham and S. Jung, Phys. Rev. D **97**, 024052 (2018).
[8] S. Hawking, Mon. Not. R. Astron. Soc. **152**, 75 (1971).
[9] B. J. Carr and S. W. Hawking, Mon. Not. R. Astron. Soc. **168**, 399 (1974).
[10] E. W. Kolb and I. I. Tkachev, Phys. Rev. Lett. **71**, 3051 (1993).
[11] E. W. Kolb and I. I. Tkachev, Astrophys. J. **460**, L25 (1996).
[12] T. Bringmann, C. Kiefer, and D. Polarski, Phys. Rev. D **65**, 024008 (2001).
[13] D. Blais, T. Bringmann, C. Kiefer, and D. Polarski, Phys. Rev. D **67**, 024024 (2003).
[14] V. Berezinsky, V. Dokuchaev, and Y. Eroshenko, Phys. Rev. D **68**, 103003 (2003).
[15] J. Diemand, B. Moore, and J. Stadel, Nature (London) **433**, 389 (2005).
[16] K. M. Zurek, C. J. Hogan, and T. R. Quinn, Phys. Rev. D **75**, 043511 (2007).
[17] M. Ricotti and A. Gould, Astrophys. J. **707**, 979 (2009).
[18] M. Kopp, S. Hofmann, and J. Weller, Phys. Rev. D **83**, 124025 (2011).
[19] E. Hardy, J. High Energy Phys. 02 (2017) 046.
[20] P. Tisserand *et al.* (EROS-2 Collaboration), Astron. Astrophys. **469**, 387 (2007).
[21] S. Calchi Novati, S. Mirzoyan, P. Jetzer, and G. Scarpetta, Mon. Not. R. Astron. Soc. **435**, 1582 (2013).
[22] R. J. Nemiroff and V. G. Bistolas, Astrophys. J. **358**, 5 (1990).
[23] P. N. Wilkinson, D. R. Henstock, I. W. A. Browne, A. G. Polatidis, P. Augusto, A. C. S. Readhead, T. J. Pearson, W. Xu, G. B. Taylor, and R. C. Vermeulen, Phys. Rev. Lett. **86**, 584 (2001).
[24] B. Carr, F. Kuhnel, and M. Sandstad, Phys. Rev. D **94**, 083504 (2016).
[25] T. T. Nakamura, Phys. Rev. Lett. **80**, 1138 (1998).
[26] R. Takahashi, Astrophys. J. **835**, 103 (2017).
[27] P. Schneider, J. Ehlers, and E. E. Falco, *Gravitational Lenses* (Springer, Berlin, 1992).
[28] R. Takahashi and T. Nakamura, Astrophys. J. **595**, 1039 (2003).
[29] Spin precession, orbital eccentricity, and nonquadrupole modes can introduce amplitude oscillations. Higher-order post-Newtonian effects can introduce a frequency-dependent amplitude scaling $\propto f^{-7/6}(1 + \Sigma_k \alpha_k f^{(k-5)/3})$; some values of $\alpha_k(m_1, m_2, s_1, s_2)$ might provide a good agreement with a lensed waveform. A more dedicated study should include these effects.
[30] For example, a relative likelihood $\langle \tilde{h}^L | \tilde{h}^L \rangle - \langle \tilde{h}^L | \tilde{h}_{\rm best-fit} \rangle^2 / \langle \tilde{h}_{\rm best-fit} | \tilde{h}_{\rm best-fit} \rangle$ more directly measuring how much lensed waveform improves best-fit can be used, where $\langle \tilde{h}^L | \tilde{h}^L \rangle$ is defined to be Eq. (7). Once we find the $\tilde{h}_{\rm best-fit}$ by minimizing the likelihood, we obtain very similar numerical results, e.g., Fig. 2. Mathematically, the minimization actually makes both observables identical.
[31] B. P. Abbott *et al.* (LIGO Scientific and Virgo Collaborations), Phys. Rev. Lett. **116**, 131103 (2016).
[32] The ringdown and merger part of waveform can non-negligibly affect SNR for heavy binaries with $\mathcal{M}_z \gtrsim 60\ M_\odot$. For this case, we normalize our inspiral-only SNR to that value in

Ref. [33] while keeping using the ratio variable ϵ defined and calculated as in text.
[33] B. P. Abbott *et al.*, Phys. Rev. D **93**, 112004 (2016); **97**, 059901(A) (2018).
[34] C. Cutler and E. E. Flanagan, Phys. Rev. D **49**, 2658 (1994).
[35] Z. Cao, L. F. Li, and Y. Wang, Phys. Rev. D **90**, 062003 (2014).
[36] L. Dai, T. Venumadhav, and K. Sigurdson, Phys. Rev. D **95**, 044011 (2017).
[37] The probability for random noise to mimic lensing distortion (on top of unlensed waveform) would be $\sim \exp(-\mathrm{SNR}^2_{\mathrm{test}}/2) \lesssim 3 \times 10^{-6}$, 0.01 for $\mathrm{SNR}_{\mathrm{test}} \geq 5, 3$, respectively. The former probability is much smaller than typical strong lensing probability shown in Fig. 3 so that $\mathrm{SNR}_{\mathrm{test}} \geq 5$ can be confidently associated to the GW lensing, whereas $\mathrm{SNR}_{\mathrm{test}} \geq 3$ can be somewhat loose.
[38] M. Dominik, E. Berti, R. O'Shaughnessy, I. Mandel, K. Belczynski, C. Fryer, D. E. Holz, T. Bulik, and F. Pannarale, Astrophys. J. **806**, 263 (2015).
[39] It is actually a complicated function of z_S, $\mathcal{M}_z$, and, etc. The total merger-rate density may grow with z_S up to $z_S \simeq 2$ [40], but heavier binaries may decrease with z_S. Considering all these dependencies is beyond the scope of this Letter, but we conservatively and conveniently assume a constant value taken from small $z_S \leq 0.1$ shown in Fig. 3 of Ref. [40].
[40] K. Belczynski, D. E. Holz, T. Bulik, and R. O'Shaughnessy, Nature (London) **534**, 512 (2016).
[41] M. Oguri, J. M. Diego, N. Kaiser, P. L. Kelly, and T. Broadhurst, Phys. Rev. D **97**, 023518 (2018).
[42] T. D. Brandt, Astrophys. J. **824**, L31 (2016).
[43] J. M. Diego *et al.*, Astrophys. J. **857**, 25 (2018).
[44] T. Venumadhav, L. Dai, and J. Miralda-Escud, Astrophys. J. **850**, 49 (2017).
[45] J. B. Munoz, E. D. Kovetz, L. Dai, and M. Kamionkowski, Phys. Rev. Lett. **117**, 091301 (2016).
[46] M. Zumalacarregui and U. Seljak, Phys. Rev. Lett. **121**, 141101 (2018).
[47] A. Gould, Astrophys. J. **386**, L5 (1992).
[48] A. Barnacka, J. F. Glicenstein, and R. Moderski, Phys. Rev. D **86**, 043001 (2012).